Precision Star Tracker Utilizing Advanced Techniques and Materials

R. F. Gates* and K. J. McAloon*
TRW Systems and Energy, Redondo Beach, Calif.

An image dissector star tracker has been developed which operates in the photon counting mode, making it possible to utilize all-digital electronics. A unique pulse processing circuit allows bright stars to be tracked as well as dim stars. Thermal mechanical stability has been greatly enhanced by fabricating a housing with graphite/epoxy composite material with a linear coefficient of thermal expansion near zero. Tests results indicate the +10 Mv stars can be acquired and tracked, while position variation with star intensity is less than 2 arcsec from +2.5 Mv to +10 Mv. The noise equivalent angle for a +8 Mv star is 3 arcsec. Polynominal correction for remaining cross-coupling and nonlinearity reduced error over a total 1° by 1° field to 1.5 arcsec (1σ).

Introduction

Recent spacecraft applications involving astronomical and Earth-pointing missions emphasize the need for attitude determination systems with arcsec accuracy. Star trackers using image dissector tubes provide high resolution instruments for determining inertial attitude, but arcsec accuracies require narrow fields of view due to the errors associated with magnetic deflection. However, narrow fields of view necessitate the tracking of very dim stars. These considerations have resulted in a requirement for a star tracker with significant improvements in accuracy, sensitivity, and dynamic range. This paper describes the design, development, and testing of a tracker to meet these requirements.

The star tracker was designed as a component of a precision attitude determination system for a three-axis-stabilized, Earth-pointed, geosynchronous satellite. The tracker is fixed to the spacecraft axes and relies on orbit motion for star availability. Figure 1 is a photograph of a developed tracker, and Table 1 lists its design parameters.

The sensitivity of the image dissector star tracker has been dramatically increased by operating in the photon counting mode. Stars as dim as +10 Mv were tracked with a 60-cm^2 optics aperture. This greater sensitivity makes a 1° by 1° field of view feasible without a decrease in star availability.

A unique pulse processing circuit, combined with the photon counting technique, allowed star magnitudes from +10 Mv to −2 Mv to be acquired and tracked without changing electronic circuitry or scaling. Position variation with star intensity was measured to be less than 2 arcsec from +10 Mv to +2.5 Mv.

Photon counting also facilitates the conversion of the search and track electronics to digital circuitry; nearly all of the analog circuits, which require adjustment during unit test and which tend to introduce electronic errors, are eliminated.

The star tracker has been tested both statically and dynamically. Static testing was completely automated and used a collimated star source with 121 separate stars in an 11 by 11 array. The array was used in determining a ten-coefficient polynomial for compensating field-of-view nonlinearities. The error after compensation was 1.5 arcsec (rms) over the entire field. Dynamic testing indicated less than 1 arcsec dynamic lag when tracking a +8 Mv star moving at geosynchronous orbit rate, 15 deg/hr. The single-sample noise (one sample per 0.1 sec) for an 8 Mv star was 3 arcsec. A ten-day boresight stability test resulted in a peak drift of 2 arcsec.

Received Dec. 29, 1975; presented as Paper No. 76-113 at the AIAA 14th Aerospace Sciences Meeting, Washington, D.C., Jan. 26-28, 1976; revision received May 10, 1976. This work was partially supported by NASA Langley Research Center under Contract NAS 1-12894.

Index Category: Spacecraft Attitude Dynamics and Control.

*Senior Staff.

Field of View/Sensitivity Consideration

The requirement for arcsec accuracy in an image dissector star tracker leads to consideration of smaller fields of view to reduce the errors associated with magnetic deflection. These errors can be separated into two types: 1) nonlinearities and cross-coupling in the magnetic fields created by the deflection coils, and 2) electronic errors.

Typical values for the magnetic field errors range from 0.2% to 1% distortion at the corners of the field of view, i.e., 7 to 36 arcsec in a 1° by 1° field. Current design practice is to calibrate the output throughout the field of view and apply a software compensation algorithm.

Electronic errors affect the current through the deflection coil. These errors can be grouped into two categories: scale factor and bias. For example, a one-arcsec stability at the edge of a 1° by 1° field of view requires a combined stability of 555

Table 1 Design parameters.

Field of view	1° by 1°
Sensitivity	10 Mv GO (6000°K)
Photodetector	
type	ITT F4012
usable photocathode area	0.5 in. diam
photocathode response (8 Mv GO)	3.6×10^{-17} A/cm^2
aperture diameter	0.010 in.
Optics	
type	Cassegrain
focal length	20 in.
aperture	60 cm^2
instantaneous field of view	103 arcsec
blur circle	< 0.003 in.
Electronics	
position output	12-bit digital word
magnitude output	12-bit digital word
data sample time	0.1 sec/axis
Functional performance	
maximum acquisition time	13.7 sec
maximum track rate	0.06° /sec
Accuracy (with FOV and temperature compensation)	
LOS to EO axis	
noise	3 arcsec (8 Mv)
fixed	1.5 arcsec
star sensitivity	0.05 arcsec/Mv
magnetic field sensitivity	0.5 arcsec/Gauss
EO axes to optical cube	
bias uncertainty	2.4 arcsec

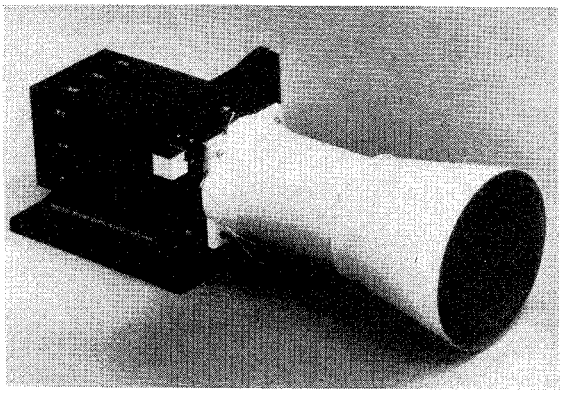

Fig. 1 Precision star tracker.

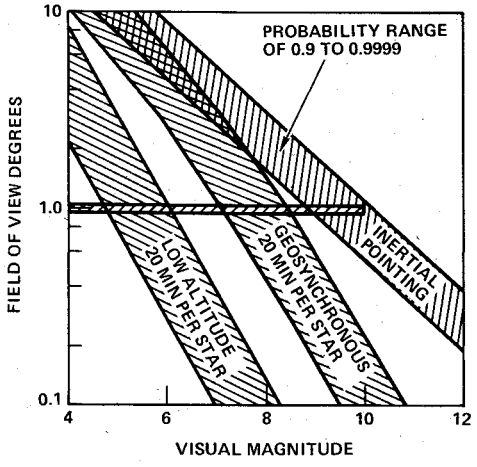

Fig. 2 Probability of one or more stars in field of view.

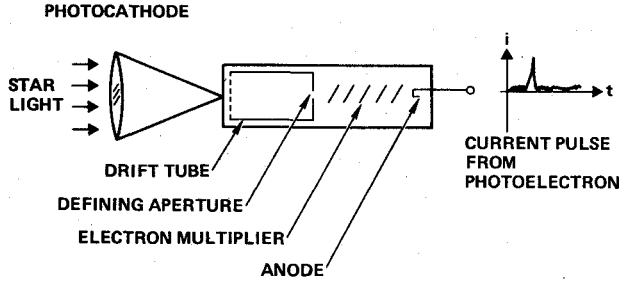

Fig. 3 Schematic of image dissector.

ppm from the deflection, focusing, and imaging circuits. A one-arcsec boresight stability requires an output bias stability of 4μA from a deflection amplifier which would give full deflection at 8 mA.

While the above error sources lead toward use of a small field of view, the complementary design parameter of star availability suggests a large field of view. Figure 2 gives star availability data[1] as a function of both field of view and star brightness. Mean star densities over the galactic sphere are used. Three cases are plotted: 1) that of a stationary, inertially pointed field of view; 2) that of a field of view moving for a 20-min period at 15°/hr., i.e., through a 5° angle; and 3) that of a field of view moving for a 20-min period at 0.06°/sec, or through 72°. The advantage of a larger field of view is that the brighter, better known stars can be used for attitude determination. For example, in a geosynchronous orbit, 8-Mv stars must be tracked by a 1° by 1° field of view to achieve the same accuracy as an 8° field of view tracking +5.3-Mv stars.

The previous tradeoffs resulted in the selection of a 1° by 1° field of view with 10-Mv sensitivity as best suited to a geosynchronous orbit. This field of view gave sufficient design margin to meet the accuracies shown in Table 1. The sensitivity is more than enough to ensure 20-min star updates.

Design Description

In the operation of a star tracker the optics system acts to focus the collimated beam of star light entering its aperture onto a small spot on the photocathode of the image dissector. The electrons emitted from this spot are focused and accelerated in a drift tube until they hit a plate with a small aperture in its middle. The magnetic deflection coils around the outside of the dissector tube deflect the electrons so that they pass through the aperture. Once through, they are multiplied in a dynode chain and finally strike the anode of the tube. This operation is schematically illustrated in Fig. 3.

An F4012RP-S20RE image dissector is used as the detector. The image dissector, dynode dividing network, focus coil, and deflection coils are potted into a triple-layer Co-Netic shield to prevent stray magnetic fields from affecting the accuracy of the tracker. The red-extended S-20 photocathode was selected as being the quietest with the best spectral response over the visual range.

Photon Counting

The ability of the image dissector to operate as a photon counter has long been known, but it is only recently that emphasis has been placed on using this characteristic in a closed-loop tracking system. The approach that has been taken is to process the photon-pulse count signal in an arithmetic processor and derive an error signal to drive the magnetic deflection coils.

As far as signal-to-noise and sensitivity are concerned, there should be no particular advantage of photon counting over an analog detection scheme.[2] But there is a practical difference in implementation when electronic circuits are considered. For instance, if only one photoelectron occurred per second, it could still be detected and counted digitally. In the analog mode this amounts to 1.6×10^{-13} A at the anode, which is lost in the dark current of 10^{-9} A. The anode dark current is due to internal leakage in the multiplier section. For this reason, photon counting is superior to the analog mode for detecting weak signals.

Since, in low-light-level conditions, electrons leave the photocathode individually, the result at the anode is a very short pulse of current related to the single electron by the gain of the multiplier.

Therefore, the peak anode pulse current is

$$I_p = 2\pi qk/\tau \qquad (1)$$

where q = charge on single electron, $=1.6\times10^{-19}$, T = pulse length, and k = multiplier gain.

The pulse length is determined by the bandwidth of the video amplifier and the stray capacitances associated with the output stages of the image dissector. The effect of the stray capacitances can be minimized by using small values of resistance in the anode circuit. Thus, with a multiplier gain of 10^6 and a pulse length of 100 nsec, the peak pulse current is 10 μA.

An anode load resistance of 1000 Ω will develop a signal of 10 mV across it. An amplifier with a bandwidth of 10 MHz needs a gain of 350 to 400 to raise this to a suitable level for use in TTL circuitry.

Search

In the search mode the deflection coils sequentially deflect electrons emitted from each of 64 by 64 equally spaced areas on the photocathode into the aperture. The areas overlap each other by the optics blur-circle size. If a star image is in a particular area, a counter which detects photon pulses will exceed a commanded threshold and switch to the track mode. This

technique will select the first star in the search raster brighter than a selected intensity.

Other search techniques which can be implemented include: 1) selection of the brightest star in the field of view, 2) continuous mapping of all stars in the field of view brighter than a selected intensity, and 3) a minisearch raster about a selected point in the field of view.

A frequent design constraint in the search mechanism is the time required to sweep the entire field of view. This time is a function of the instantaneous field of view and the dwell time during which photon pulses are counted. The instantaneous field of view is approximately equal to the tube aperture divided by the focal length of the optics. It is desirable to keep the instantaneous field of view small because it affects the accuracy obtainable during track. On the other hand, as it becomes smaller, the number of dwell positions in the field of view becomes greater. The dwell time at each position must be long enough to distinguish the star photon count from the background noise with a high statistical probability. In a realistic application the background noise is nearly entirely due to reflected light entering the shade or from stellar background.

In the implemented design a 103-arcsec instantaneous field of view is used to scan 64 by 64 equally spaced areas in the field of view. The dwell time at each of the 4096 areas is 3.3 msec, or 13.7 sec to scan the total field of view.

Track

In the track mode the deflection coils provide an average deflection of the photoelectrons such that they continuously pass through the aperture. The coil currents are then used as a measure of the star position relative to the boresight axes.

Spatial modulation of the photoelectron beam relative to the aperture is used to keep the average beam position centered in the aperture. A number of modulation techniques are possible with the photon counting technique. Figure 4 illustrates three possible variations. In all the techniques, signal information content is derived from the photon count rate at different star positions relative to the aperture. The techniques can be grouped into two categories: 1) those whose information content is primarily a function of the aperture size, and 2) those whose content is primarily a function of the star blur-circle size. The cruciform is an example of the former, while the four-sides and four-corners techniques are examples of the latter.

The cruciform is used in the implemented design for two reasons: 1) to provide a wide dynamic range in star intensity when combined with a unique circuit implementation, and 2) to make the tracking loop gain independent of the star blur-circle size. Although this technique does not result in minimum sensor noise, in an attitude determination application the noise parameter is not a major error source.

One of the drawbacks of a photon counting scheme is the limited dynamic range of the signal intensity which can be tracked. Signal noise and loop bandwidth requirements fix the minimum photon pulse rate. The finite pulse width of each pulse, fixed by tube stray capacitances, will determine the maximum pulse rate which can be detected. Given a star tracker designed to track very dim stars, it is advantageous to also be able to track bright stars if they occur, since their inertial position is generally better known. Consequently, a unique video pulse synchronizer circuit was devised to operate in conjunction with a cruciform pattern to give a dynamic range of from $>10{,}000$ to 1, or over ten star magnitudes. This circuit accommodates operation of the image dissector tube in either the pulse mode or the continuous current mode with no significant boresight shifts with star intensity.

The second reason for using the cruciform technique is to make the track loop gain depend on the tube aperture size and, consequently, to make it fixed. The transfer function of the cruciform technique, i.e., signal out versus average star position in, is independent of the blur-circle size provided that

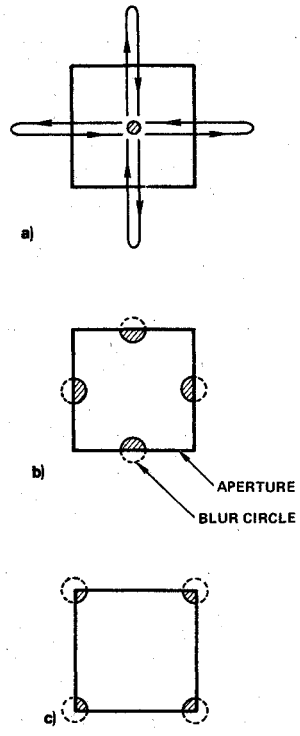

Fig. 4 Spatial modulation techniques: a) cruciform; b) four sides; c) four corners.

the circle remains smaller than the aperture. This fact allows greater flexibility in specification of the optical system aberrations and magnetic focusing requirements, and in star simulation. Also, a fixed loop gain means that the dynamic lag in tracking a moving star is analytically predictable and compensatable.

The cruciform technique yields pulse width modulated information. Signal waveforms are shown in Fig. 5. In order to make the transfer function independent of star magnitude, the error signal is calculated as the ratio of up minus down counts divided by up plus down counts. Each axis is updated every 0.1 sec.

Digital Electronics

The availability of a photon pulse signal in the search mode facilitates the nearly complete conversion of the search and track circuitry to a digital mechanism. Except for the pulse amplifier and the coil deflection amplifiers, all other circuitry is digital or quasidigital.

The design is implemented with integrated digital circuits. Up-down counters count the photon pulses in both search and track. Counters drive the digital-to-analog converters to provide both the search sweep and the cruciform patterns. An arithmetic processor derives the track loop error signal. The rest of the circuits consist of clock generators and gating logic.

An added capability of the digital design is the ability to increase the frequency of the main clock driving both the search and track electronics. Three separate frequencies are commandable; the effects on the search and track timing are shown in Table 2. The normal clock position is C and the design parameters in Table 1 reflect this frequency.

Table 2 Digital electronics timing

Clock position	Search Dwell time	Search Frame time	Track Loop sample time
A	0.8 msec	3.4 sec	26.7msec
B	1.7 msec	6.8 sec	53.3 msec
C	3.3 msec	13.7 sec	106.7 msec

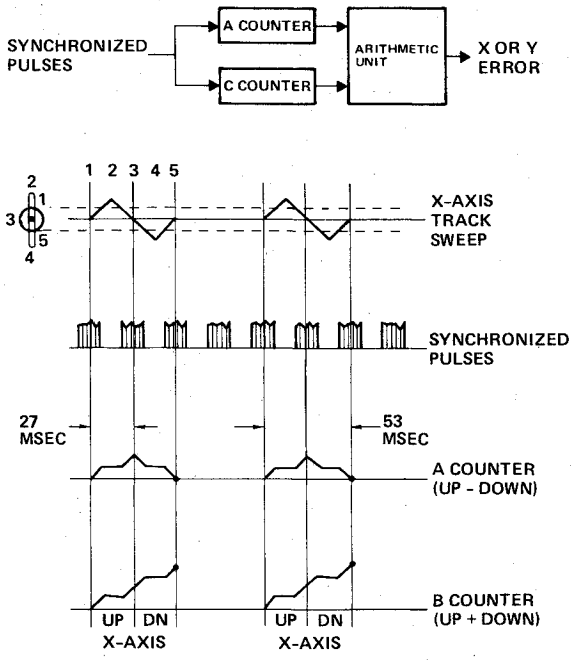

Fig. 5 Cruciform signals.

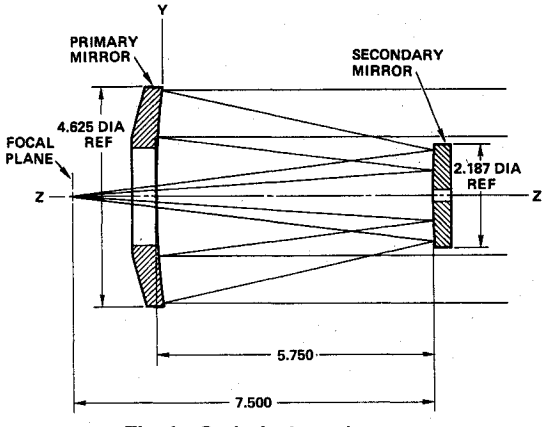

Fig. 6 Optical schematic.

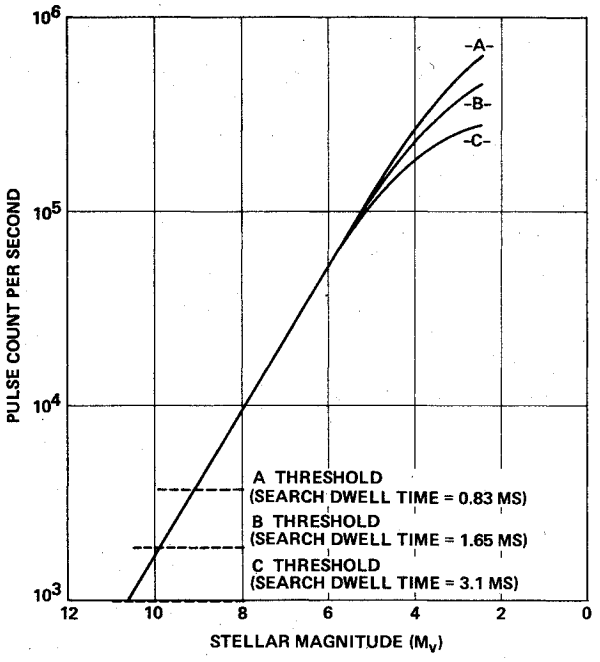

Fig. 7 Sensitivity.

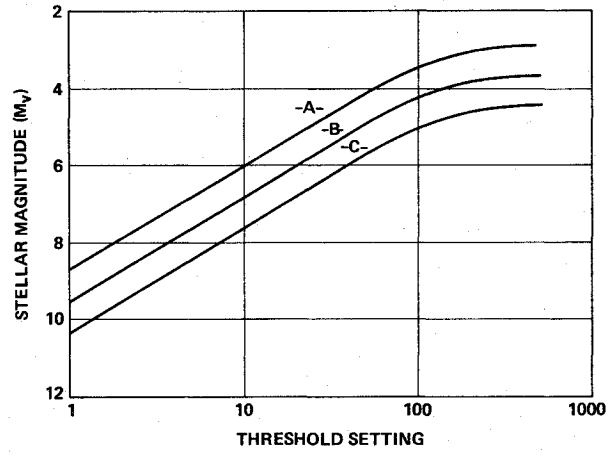

Fig. 8 Command threshold sensitivity.

With the rapid development of microprocessor technology, the next stage now in process in star tracker development is the conversion of the integrated circuits to a microprocessor. It is highly feasible to use a microprocessor to implement the photon counting technique. The large percentage of digital circuits involved will mean a significant decrease in number of parts, together with an attendant reduction in electronics assembly and checkout time. Perhaps equally important is the design versatility associated with the microprocessor. Some of the many design parameters which can be implemented in software are: the search technique, the search rate, adaptive thresholding, track loop sample time and gains, dynamic lag compensation, field of view compensation, and output noise filtering.

Mechanical Housing

One of the most persistent problems in the design of electro-optical instruments for use in space is the thermal mechanical stability of the boresight null axis. This axis is defined by 1) the principal point of the principal plane of the optics, and 2) the point on the detector at which a star image indicates zero position output. The spacing between those two points, as well as the orientation of a line through them relative to the mounting surfaces, must be maintained constant over the temperature range which the tracker will be subject to. A search was commenced for a material that would have near zero coefficient of linear thermal expansion. This effort resulted in a housing design using a graphite/epoxy composite material which was rigid enough to support the tracker and which provided excellent thermal stability.

The graphite/epoxy material is made up of both linear and random fibers to utilize the maximum effectiveness of each. The resultant material has a measured linear coefficient of thermal expansion (LCTE) of only -0.25×10^{-6} in./in.°C, nearly 100 times less than aluminum. One of the interesting features of the material is that the LCTE can be tailored over a fairly broad range to fit most requirements. The optical housing was vacuum baked and vacuum deposited with a conformal coating to prevent moisture absorption deformation, prior to having the aluminum screw inserts bonded in place. The finished housing assembly was slightly lighter than an equivalent aluminum housing.

Optics Design

Keeping the 1° by 1° field of view within the .5-in.-diam quality area resulted in a 10-in. focal length optical system. Since it was desirable to keep the sensor length as short as possible, a reflective cassegrain design was selected. Sensitivity requirements dictated a 60-cm^2 clear aperture which, in turn, set the diameter of the primary mirror. Figure 6 is a

schematic layout of the system that evolved. Because of the secondary obscuration, the center of the primary was removed and the primary mirror was mounted directly to the tube assembly, making it possible to keep the back focal length reasonably short. The optical elements were fabricated from Cervit. The blur circle over a 1.5° field was less than 1 mil.

Test Results

Star tracker testing was performed in two separate facilities. The Unit Test Facility was used to assist in the final assembly of the star tracker and to perform certain static tests on the unit. The System Test Facility was used to test the tracker response to stars moving through the field of view at different rates and to carry out long-term boresight stability tests.

Unit Tests

The unit tests on the tracker consisted of sensitivity, threshold, linearity, stability, null stability with star brightness, and noise equivalent angle.

Sensitivity

The sensitivity was determined by using NASA/Goddard standard star source #10 as a reference.

The photocathode current per square centimeter of optical aperture is given by

$$I_p = \left(\frac{D_1}{D_2}\right)^2 S_p\, T \int_{300}^{800} S(\lambda)\, H(\lambda)\, d\lambda$$

$$= 0.48 \times 10^{-14}\ \text{A/cm}^2 \qquad (2)$$

where $D_1 = 7.5$ m, the distance at which the Goddard source was calibrated; $D_2 = 2.34$ m, the focal length of the collimating lens; $S_p = 0.064$ A/W, the peak response of the S-20 photocathode; $T = 0.8$, the transmittance of the collimating lens; $S(\lambda)$ = the relative spectral response of the photocathode; and $H(\lambda)$ = the spectral energy distribution of the Goddard star source.

Forbes and Mitchell[3] list, for an S-20 photocathode, a photocathode current of 0.488×10^{-13} A/cm^2 for Alphas Bootes (Arcturus), a K2 spectral type star with a visual magnitude of -0.05. Thus we can safely say, since our output is ten times less, that the Goddard source in our test setup is equivalent to a +2.5 K2 star.

The signal strength output was recorded at each of the three clock positions, A, B, and C. Various neutral density filters were then inserted and the signal strength output recorded. The data obtained are shown in Fig. 7. The difference in the knee of each curve is due to the clock frequencies which set the upper count rate.

Command threshold sensitivities were measured, using an LED source, by increasing the current through the LED until acqusition occurred at each commanded threshold. The photon-pulse count was recorded and the magnitude determined from Fig. 7 The result is plotted in Fig. 8. The threshold setting refers to the 10-bit command which sets the count in the acquisition pulse counter which must be exceeded before acquisition occurs.

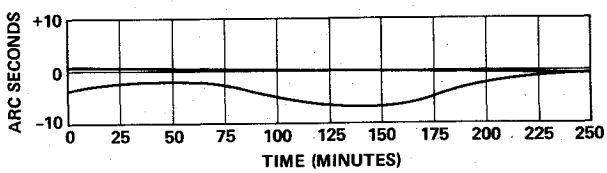

Fig. 9 Warmup drift.

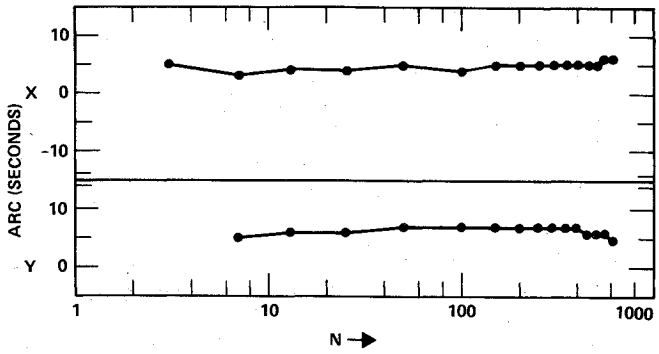

Fig. 10 Position shift with star brightness.

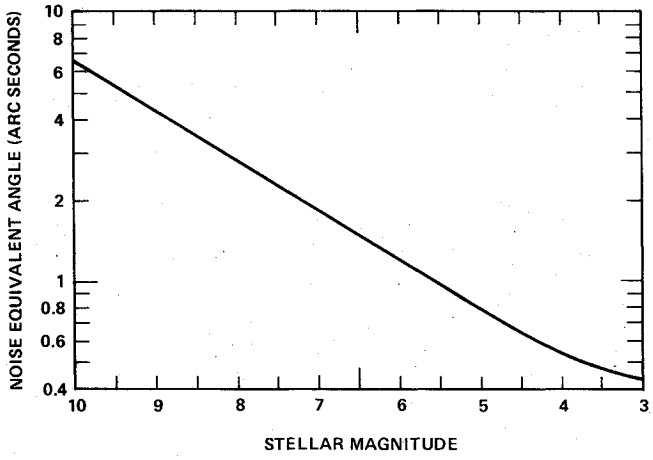

Fig. 11 Noise equivalent angle.

Linearity

The test setup to measure linearity uses a matrix of 121 LED's behind a photoreduced aperture plate located at the focal plane of a collimating lens. The LED's can be turned on manually from the control console, or they can be automatically sequenced by the HP 9100 calculator. In the automatic sequencing mode, the number of samples taken at each position can be set into the HP 9100, and then the mean and standard deviation determined.

The tracker had been originally set up so that star 6,6 read 0,0 and the axis had been aligned so that the x axis was parallel to the mounting plate to within 5 arc sec.

Field-of-View Compensation

The calibration data from the 121 equally spaced stars was fit in the least-squares sense to the following polynomial:

$$\hat{x} = a_{x_0} + a_{x_1} u + a_{x_2} u^2 + a_{x_3} u^3 + a_{x_4} v + a_{x_5} v^2 + a_{x_6} v^3 + a_{x_7} uv + a_{x_8} u^2 v + a_{x_9} uv^2 \qquad (3)$$

$$\hat{y} = a_{y_0} + a_{y_1} v + a_{y_2} v^2 + a_{y_3} v^3 + a_{y_4} u + a_{y_5} u^2 + a_{y_6} u^3 + a_{y_7} vu + a_{y_8} v^2 u + a_{y_9} vu^2 \qquad (4)$$

where $\hat{x}$, $\hat{y}$ = estimated star position, and u, v = star tracker 12-bit binary output (smoothed). The standard deviation of the errors after application of the polynomial fit to the 121 stars was 2 arcsec in each axis.

Stability

Warmup stability over a 4-hr period is shown in Fig. 9. The vertical axis shows a cyclic drift which has been attributed to the air conditioning effect on the 5-m steel optical bench.

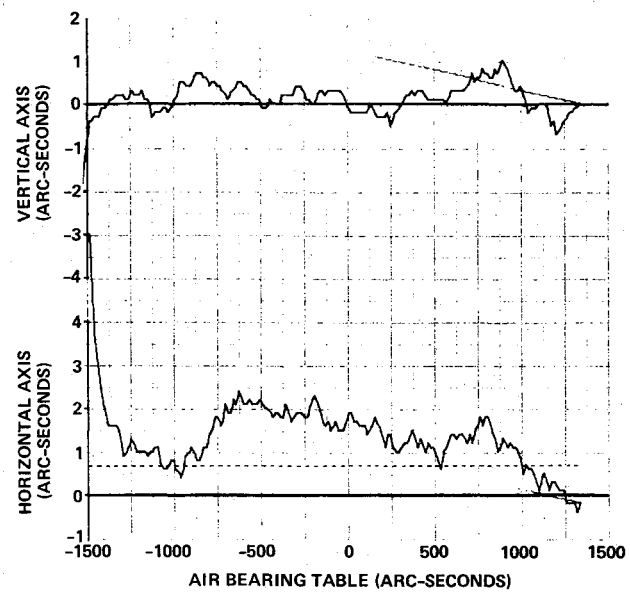

Fig. 12 Dynamic accuracy.

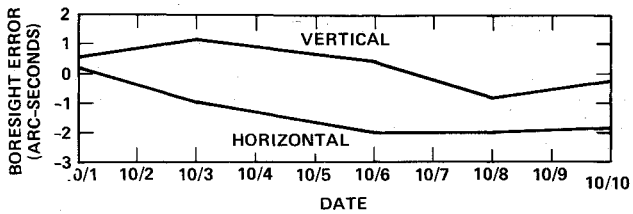

Fig. 13 Long-term boresight accuracy.

Earlier analog work indicated a null shift with star brightness, so a test was run to see if it occurred in the photon counting tracker. Figure 10 shows the results of this test. The range of equivalent stellar magnitudes covered was +2.5 to +10. The tests indicate that the null stability with respect to star brightness is very good.

Noise Equivalent Angle

The noise equivalent angle was automatically printed out during the running of the sensitivity tests. The results are shown in Fig. 11.

System Tests

The System Test Facility is designed to test both attitude determination systems and their individual components: star trackers and gyros. The facility consists of a dark room with an isolated seismic pad, a control area, and a digital computer area.

Three stars at different elevations can be moved in a horizontal direction through the tracker field of view at any commanded rate. Star direction relative to the star tracker optical cube is known to within 1 arcsec at any position within the field of view.

Two types of tests were performed in this facility: 1) dynamic field-of-view tests and 2) static long-term boresight drift tests. In the dynamic tests, stars were moved through the field of view at Earth rate to simulate the optical environment in geosynchronous orbit for a strapdown star tracker mounted on a three-axis-stabilized, Earth-pointed satellite. In the boresight test, the direction of the electro-optical boresight of the tracker relative to its optical cube was measured over a ten-day period to determine its drift.

Figure 12 illustrates the star tracker dynamic accuracy for a star moving at 15°/hr horizontally through the field of view. The difference is plotted between the star tracker indicated position, compensated with the polynomial expression, and the star true position. The star moved from right to left through the figure, and a 20-sec first-order filter was used to smooth the error signal. The track loop dynamic lag appears in the horizontal output. The dashed line indicates the analytical value of 0.7 arcsec. The indicated error is due to three factors: 1) the dynamic response of the track loops, 2) the polynomial fit residues, and 3) tracker output white noise driving the 20-sec time-constant filter. From an ensemble of 48 star transients, the error was consistently less than 3 arcsec in either axis. The stability of the star tracker electro-optical boresight relative to the optical cube on the tracker is shown in Fig. 13. The boresight position was measured five times in a ten-day period.

References

1. Allen, C. W., *Astrophysical Quantities,* University of London, Athlone Press, 1963, p. 234.

2. Rolfe, J. and Moore, S. E., "The Efficient Use of Photomultiplier Tubes for Recording Spectra," *Applied Optics,* Vol. 9, 1970, p.1.

3. Forbes, F. F. and Mitchell, R. E., "Stellar Photometric Data for Six Different Photocathode Materials and the Silicon Detector," Table I, No. 141 *Communications of the Lunar and Planetary Laboratory,* University of Arizona, Tucson, Dec. 1963.